Available online at www.sciencedirect.com
SCIENCE DIRECT®
Journal of Structural Biology 147 (2004) 302–314
Journal of Structural Biology
www.elsevier.com/locate/yjsbi

Global ribosome motions revealed with elastic network model

Yongmei Wang,[a] A.J. Rader,[b] Ivet Bahar,[b] and Robert L. Jernigan[c,*]

[a] *Department of Chemistry, University of Memphis, Memphis, TN 38152-3550, USA*
[b] *Department of Molecular Genetics and Biochemistry, Center of Computational Biology and Bioinformatics, School of Medicine, Health Sciences, University of Pittsburgh, Pittsburgh, PA 15261, USA*
[c] *Department of Biochemistry, Biophysics and Molecular Biology, Laurence H. Baker Center for Bioinformatics and Biological Statistics, Iowa State University, Ames, IA 50011, USA*

Received 7 November 2003, and in revised form 13 January 2004
Available online 27 February 2004

Abstract

The motions of large systems such as the ribosome are not fully accessible with conventional molecular simulations. A coarse-grained, less-than-atomic-detail model such as the anisotropic network model (ANM) is a convenient informative tool to study the cooperative motions of the ribosome. The motions of the small 30S subunit, the larger 50S subunit, and the entire 70S assembly of the two subunits have been analyzed using ANM. The lowest frequency collective modes predicted by ANM show that the 50S subunit and 30S subunit are strongly anti-correlated in the motion of the 70S assembly. A ratchet-like motion is observed that corresponds well to the experimentally reported ratchet motion. Other slow modes are also examined because of their potential links to the translocation steps in the ribosome. We identify several modes that may facilitate the E-tRNA exiting from the assembly. The A-site t-RNA and P-site t-RNA are found to be strongly coupled and positively correlated in these slow modes, suggesting that the translocations of these two t-RNAs occur simultaneously, while the motions of the E-site t-RNA are less correlated, and thus less likely to occur simultaneously. Overall the t-RNAs exhibit relatively large deformations. Animations of these slow modes of motion can be viewed at http://ribosome.bb.iastate.edu/70SnKmode.

Keywords: Translocation; Dynamic transitions; Molecular machine; Global motion; Normal mode analysis

1. Introduction

The ribosome is the large RNA–protein assembly that decodes the messenger-RNA and synthesizes the proteins in accord with the sequence of the mRNA. It is comprised of two subunits of unequal size, which together form the complete ribosome. The large 50S subunit in prokaryotes is composed of a 23S rRNA, a 5S rRNA, and 34 proteins; whereas the small 30S subunit is formed from a 16S rRNA and 21 proteins. Together these two subunits form the 70S ribosome. The main catalytic function of the ribosome is performed by rRNAs, not by proteins; hence the ribosome is actually a ribozyme (Ban et al., 2000). The 30S subunit binds mRNA and the anticodon end of the tRNAs and is involved in decoding the mRNA. The 50S subunit interacts with the amino acid carrying ends of the tRNAs and catalyzes peptide bond formation. During protein synthesis, the whole assembly undergoes a series of highly coordinated movements necessary for the efficient translation of the messenger-RNA into proteins. The movements include several translocation steps: translocation of the A-site tRNA to the P-site and the P-site tRNA to the E-site, together with the translocation of the messenger-RNA by exactly one codon. Many attempts are underway to develop a more detailed understanding of the translocation steps in the ribosome.

Cryo-electron microscopy (cryo-EM) of the ribosome has provided an initial understanding of the steps involved during protein synthesis (Agrawal et al., 1999; Frank and Agrawal, 2000; Frank et al., 1999; Valle et al., 2002; VanLoock et al., 2000; Wriggers et al., 2000). The translocation within the ribosome is achieved

* Corresponding author. Fax: 1-515-294-3841.
E-mail address: jernigan@iastate.edu (R.L. Jernigan).

1047-8477/$ - see front matter © 2004 Elsevier Inc. All rights reserved.
doi:10.1016/j.jsb.2004.01.005

with the binding of elongation factors (EFs) and GTP hydrolysis. By analyzing three-dimensional cryo-EM snapshots of the 70S ribosome at various functional states, Frank and Agrawal (2000) have observed ratchet-like rotations of the 30S subunit relative to the large 50S subunit during translocation. Many insights have also been gained regarding the possible sequential steps during the translocations, although details have not been completely resolved (Agrawal et al., 2000; Noller et al., 2002). Additional methods such as NMR and fluorescence resonance energy transfer (FRET) are providing some further details (Lynch et al., 2003).

The X-ray crystal structure of the 30S subunit from the *Thermus thermophilus* has been determined by Wimberly and co-workers (Carter et al., 2000; Wimberly et al., 2000) to 3 Å resolution and independently by Schluenzen et al. (2000) to 3.3 Å resolution. Ban et al. (2000) have determined the crystal structure of the 50S subunit from *Haloarula marismortui* to 2.4 Å. Recently, the crystal structure of the entire assembly of the 70S ribosome from the *T. thermophilus* has been reported by Yusupov et al. (2001). These crystal structures have confirmed the earlier suggestion that the rRNAs provide the catalytic function of the ribosome. The rRNAs also give the overall shape of the structure and the proteins act as fillers, being inserted mostly in the exterior at niches between parts of the rRNAs.

The cooperative motions in the ribosome are not usually accessible with conventional molecular simulations. Coarse-grained elastic network models such as the Gaussian network model (GNM; Bahar and Jernigan, 1999; Bahar et al., 1997a,b, 1998, 1999; Haliloglu et al., 1997) or the anisotropic network model (ANM; Atilgan et al., 2001) after the uniform elastic network (EN) model originally proposed by Tirion (1996) have proven to be extremely useful in the study of global motions of a large number of different proteins (Bahar et al., 1999; Isin et al., 2002; Keskin et al., 2002a,b; Ma and Karplus, 1997; Tama and Brooks, 2002; Tama et al., 2002; Temiz and Bahar, 2002) and have been validated by numerous comparisons with crystallographic temperature factors. The low frequency normal modes obtained in GNM or ANM analysis often can be correlated with the functionally important conformational motions of proteins. Therefore, by examining only a few slowest normal modes, one can gain a good understanding of the cooperative motions for a particular enzyme or RNA. Applying such simplified normal mode analysis (NMA) to the reported X-ray structures of the ribosome can aid us to better understand the cooperative motions within the ribosome.

2. Methodology

The GNM and ANM methods have been described earlier (Atilgan et al., 2001; Haliloglu et al., 1997). In both methods, the structures are coarse-grained by taking only one site per residue (or two sites per nucleotide) and imposing a simple harmonic potential between the sites that are sufficiently close to lie within a cutoff distance R_c. By this simplification, the structure is reduced to a set of beads (assumed to have the same masses) connected with harmonic springs, or simply an EN. In the GNM model, the potential between sites i and j is given by

$$V_1(\vec{\boldsymbol{R}}_{ij}) = \frac{1}{2}\gamma\left(\vec{\boldsymbol{R}}_{ij} - \vec{\boldsymbol{R}}^0_{ij}\right)^2 H(R_c - R_{ij}) = \frac{1}{2}\gamma(\Delta\vec{\boldsymbol{R}}_{ij})^2 H(R_c - R_{ij}), \quad (1)$$

where $H(x)$ is the Heaviside step function equal to 1 if $x > 0$, and zero otherwise, $\vec{\boldsymbol{R}}_{ij}$ is the distance vector between the ith and jth sites, R_{ij} is its magnitude, the superscript 0 refers to the value in the reference (equilibrium/native) structure, $\Delta\vec{\boldsymbol{R}}_{ij}$ is the instantaneous fluctuation in $\vec{\boldsymbol{R}}_{ij}$ away from its reference position, $(\Delta\vec{\boldsymbol{R}}_{ij})^2$ is found from the scalar product $(\Delta\vec{\boldsymbol{R}}_{ij}\cdot\Delta\vec{\boldsymbol{R}}_{ij})$, and γ is the force constant. In the ANM, the potential is defined as a function of inter-residue distances as

$$V_2(\vec{r}_{ij}) = \frac{1}{2}\gamma(R_{ij} - R^0_{ij})^2 H(R_c - R_{ij}). \quad (2)$$

Note that in the ANM the potential depends on inter-residue distances, exclusively, whereas in the GNM the potential depends on the *direction* of inter-residue distances, in addition to their distances, because the GNM potential is a function of the inter-residue distance 'vectors.' As a result, the fluctuations in the three Cartesian directions in the GNM model are equal and are not coupled, hence the fluctuations are isotropic. The fluctuations in the three Cartesian directions in the ANM model are coupled and are not equal, the overall fluctuations are anisotropic.

The reference structure is taken as the reported X-ray crystal structure. The overall potential V of the network is found by summing over all interaction pairs, V may be expressed in concise form as

$$V = \frac{1}{2}\sum_i\sum_j \frac{\partial^2 V}{\partial\Delta\boldsymbol{R}_i\Delta\boldsymbol{R}_j}\Delta\boldsymbol{R}_i\Delta\boldsymbol{R}_j = (\gamma/2)\{\Delta\mathbf{R}^{\mathrm{T}}\}\boldsymbol{H}\{\Delta\mathbf{R}\}, \quad (3)$$

where $\{\Delta\boldsymbol{R}\}$ is the $3N$-dimensional fluctuation vector $\Delta\boldsymbol{R} = \mathrm{column}(\Delta\boldsymbol{R}_1, \Delta\boldsymbol{R}_2, \Delta\boldsymbol{R}_3, \ldots, \Delta\boldsymbol{R}_N)$ of the components ΔX_i, ΔY_i, and ΔZ_i of $\Delta\boldsymbol{R}_i$ for all N nodes, the superscript T denotes the transpose (i.e., $\Delta\boldsymbol{R}^{\mathrm{T}} = \mathrm{row}(\Delta\boldsymbol{R}_1, \Delta\boldsymbol{R}_2, \Delta\boldsymbol{R}_3, \ldots, \Delta\boldsymbol{R}_N)$, and $\boldsymbol{H}$ is the $3N \times 3N$ Hessian matrix (ANM; Atilgan et al., 2001) and it reduces to $\boldsymbol{\Gamma}\otimes\boldsymbol{E}$ in GNM, where $\boldsymbol{\Gamma}$ is $N \times N$ connectivity/Kirchhoff matrix (GNM), $\boldsymbol{E}$ is the 3×3 identity matrix, and $\otimes$ designates the direct product (Bahar et al., 1998).

The main difference between the GNM and ANM lies in the dynamic quantities that are elucidated in the two

methods. GNM characterizes the '*sizes*' of fluctuations, only, which may be decomposed into $N-1$ mode contributions; ANM, on the other hand, determines the $3N$ components, and thereby the '*directions*' of the fluctuation vector. ANM is more informative since the directionalities of the motions can be extracted. However, the GNM potential, which depends on the orientation and the distance between residues, is a more realistic description of the energy landscape near the global minimum where the original (native) state lies. Earlier studies show that GNM results are more robust, and are preferably resorted to for evaluating the *mean-square fluctuations* and the *squared displacements* in low frequency modes (Atilgan et al., 2001); whereas for assessing the *directions* of fluctuations or *mechanisms* of global modes, ANM is needed. GNM has the further advantage of being computationally 3^3 times faster than ANM, as the time-limiting step of computations—the decomposition of $\boldsymbol{\Gamma}$ (GNM) or $\boldsymbol{H}$ (ANM) scales with the third power of the dimension of the matrix to be diagonalized. In order to determine the mechanism of ribosome function, we apply the ANM method. Not withstanding, we resort to GNM results for verifying the consistency of the ANM modes with regard to the more limited but more accurate GNM predictions, whenever applicable.

We performed ANM analysis on the structure of the 30S subunit reported by Wimberly et al. (2000) (PDB code 1J5E), the 50S subunit reported by Yusupov et al. (2001) (PDB code 1GIY), and the 70S ribosome structure reported by Yusupov et al. (2001) (PDB code 1GIX and 1GIY). The 30S subunit by Wimberly et al. contained full coordinates for the rRNAs and the proteins. We therefore used two interaction sites per nucleotide, one on the P atom and one on O4* atom of the rRNAs, and one interaction site per amino acid on the C^{α} atom, as in earlier GNM analysis (Bahar et al., 1998). The cutoff distance for interaction is taken as 15 Å. The dimensions of the matrices to be diagonalized are $16\,266 \times 16\,266$ for the 30S subunit and $29\,238 \times 29\,238$ for the 70S. Complete conventional diagonalization of such large matrices is not possible. We used the software BLZPACK developed by Marques and Sanejouand (1995). This software allowed us to determine a specified number of eigenvalues and the corresponding eigenvectors for the matrix. This is a rapid procedure; for example for the 30S subunit, it only requires about 3 min of CPU time on a SGI Origin 2400 to determine the first 100 slowest normal modes. For the 70S unit, the CPU time remains below 1 h, but large memory is required. The 70S structure reported by Yusupov et al. contained only the P atoms of the rRNAs and C^{α} atoms of the proteins, except the three tRNAs which had their full atomic coordinates. Therefore, we used one interaction site on the P atom per nucleotide of the rRNAs and tRNAs and one interaction site on C^{α} atom of the proteins. The cutoff distance used between the C^{α}–C^{α} atoms was still 15 Å, but the cutoff distance between P–P and P–C^{α} atoms was increased to 24 Å. This follows the correspondence we have observed for increasing the cutoff distance when there are fewer sites (Doruker et al., 2002). The exact cutoff distance used does not significantly affect the results, provided that the strength of the interactions, accounted for by the spring constant, is maintained (Doruker et al., 2002).

The eigenvector $\boldsymbol{u}(i,k)$ determined for the kth normal mode in ANM specifies the displacement vector induced by the kth mode on the ith site in the Cartesian coordinates, Δx_i, Δy_i, and Δz_i. The motions of the slow modes have been animated and visualized using the visual molecular dynamics program (VMD; Humphrey et al., 1996). The mean-square fluctuation in the position of ith residue is calculated according to:

$$\left\langle \Delta R_i^2 \right\rangle = \sum_k \frac{|\boldsymbol{u}(i,k)|^2}{\lambda(k)}, \tag{4}$$

where $\lambda(k)$ is the eigenvalue of the kth normal mode (Bahar et al., 1997a) and the summation is performed over the 100 dominant (slowest) modes determined by BLZPACK. The slow modes play a dominant role in the fluctuation dynamics, because their contributions to the mean-square fluctuations scale with the inverse eigenvalue (see Eq. (4)). The distribution of fluctuations calculated using Eq. (4) can be directly compared with that indicated by the experimental B-factors.

Another useful quantity to be utilized is the measure of deformation energy for each residue, defined by Hinsen (1998) and Hinsen et al. (1999) and modified by us to describe the contribution of each mode k as

$$D_i(k) = \sum_{j=1}^{n_{ci}} \frac{1}{2}\gamma\left(|\vec{\boldsymbol{R}}_{ij}^0 + \Delta\vec{\boldsymbol{R}}_j(k) - \Delta\vec{\boldsymbol{R}}_i(k)| - |\vec{\boldsymbol{R}}_{ij}^0|\right)^2 / N\lambda(k), \tag{5}$$

where n_{ci} is the number of sites connected to the ith site, defined by the cutoff distance R_c. We have included a weighting factor, $1/\lambda(k)$, in the above definition because the amplitude of motion is inversely proportional to the square root of the eigenvalue. The sum of $D_i(k)$ over all sites gives the overall deformation energy induced by the kth mode and remains constant for all the modes.

The distribution of deformation energy over the interaction sites gives a measure of the rigidity of the structure at each site and also serves to distinguish between a site that is participating in a rigid body motion or in an internal structural change. If a site moves together as a part of the rigid body motion, then although $\langle \Delta R_i^2 \rangle$ is non-zero and can be large, D_i will be small since in rigid body motion the distances between sites are not changed. Also, if a motion of the protein consists of rigid structural domains moving relative to another, then coloring residues according to D_i will usually reveal

the flexible regions linking the rigid domains, such as the hinge sites. Therefore, this provides an informative view of domain motions (Hayward and Berendsen, 1998; Hayward et al., 1997; Krebs et al., 2002; Wriggers and Schulten, 1997).

In the GNM/ANM calculations γ is usually left as an adjustable parameter whose value is adjusted to match the average value of the experimental B-factors over all residues for the examined protein. The absolute value of γ does not affect the distribution of fluctuations, but uniformly (and linearly) rescales all residue fluctuations. A recent comparison (Kundu et al., 2002) of X-ray crystallographic B-factors with GNM predictions for 113 high-resolution PDB proteins indicated that on the average the value $k_B T/\gamma = 0.87 \pm 0.46\,\text{Å}^2$ (or $\gamma = 0.69\,\text{kcal/(mol Å}^2)$ at $T = 300\,\text{K}$) with $R_c = 7.3\,\text{Å}$ optimally reproduces experimental data. In the present study, we will not specify any γ value, but rather report the results per unit value of γ (or $\gamma = 1\,\text{kcal/(mol Å}^2)$). The calculated $\langle \Delta R_i^2 \rangle$ and D_i will thus be reduced, dimensionless numbers. The absolute amplitude of motion in each normal mode is also arbitrary and we choose an appropriate amplification factor so as to make the motions more visible. We essentially focus on the distributions and mechanisms of motions induced in different modes, which are robust and uniquely defined by the three-dimensional architecture of the ribosome.

The prediction of deformability of residues by ANM is weighted by the amplitude of motions in a particular mode. This may not provide a complete view of the flexibility of residues. An alternative measure of the flexibility/rigidity of the structure is the flexibility index calculated with the FIRST software (Jacobs et al., 2001; Rader et al., 2002). Although similar to the elastic network used in the GNM/ANM, the FIRST software (Jacobs et al., 2001) models the structure as a constraint network where the nodes are connected by rigid bars instead of springs. In this model bond torsional rotations are the only available degrees of freedom. FIRST uses a full atomic description of the structure to define the constraint network. The predictions of flexibility by FIRST will be compared with that by ANM to assure the consistency of our results.

The calculations using FIRST were completed independently on the 30S ribosomal subunit from *T. thermophilus* (PDB code 1J5E) and the 50S ribosomal subunit from *H. marismortui* (PDB code 1JJ2) which have resolutions of 3.05 and 2.4 Å, respectively. All proteins chains were included in the calculations but waters and hetero atoms were removed. Polar hydrogen atoms were added using the program Reduce (Word et al., 1999). Covalent bonds, hydrogen bonds, salt bridges, and hydrophobic interactions between pairs of carbon atoms separated by less than 3.5 Å are used to define the constraints (Rader et al., 2002). FIRST identifies each bond as either flexible (rotatable) or rigid (non-rotatable), based on the accessibility of rotational degrees of freedom. Groups of atoms connected to each other via rigid bonds form rigid clusters, while those connected via rotable bonds form flexible regions. The locations of these rigid and flexible bonds are then mapped onto the 3D structure of the protein for visualization and comparison.

Recently, Tama et al. (2003) have also performed a normal mode analysis on the same structure of the 70S ribosome. They used the same method as our ANM analysis, except they have applied the rotation–translation block method (RTB; Tama et al., 2000) to project the Hessian matrix to blocks of atoms of rigid structures, thus to reduce the size of the matrix required for diagonalization. We will see that their results about the large domain motions agree with ours, however, some of the details of the structural re-arrangement revealed in their studies differ from ours, perhaps due to the usage of RTB method in their study.

3. Results and discussion

3.1. Motions in the 30S subunit

Fig. 1A presents the structure of the 30S subunit viewed from its interface with the 50S subunit, color-coded according to the deformation energy averaged over the first 10 slowest modes. The whole structure consists of the head and body with important landmarks such as the beak, shoulder, platform, and the spur. The spur and beak have large deformation energy in all modes and high flexibility because they are located at the periphery of the structure. The other residues with large deformation energy are located around the neck that connects the head and body. These residues divide the 30S unit into two dynamic domains, the head and the body. The head is somewhat more rigid than the body. The motion of the 30S unit in these slow modes is comprised of the relative motion of the head with respect of the body.

Fig. 1B shows the flexible residues found in FIRST. Several of the most flexible regions indicated in Fig. 1B correspond nicely with the regions identified as most deformable in Fig. 1A. Most pronounced is that of the beak and spur regions identified by both methods to be very flexible. There are additional highly flexible regions in the interface between the head and body domains identified by both methods. In both methods, the bulk of the rRNA forms a large rigid and stable substrate shown in blue. It is interesting to note that both methods indicate some of the sites around the neck being flexible. These sites are important for the function of the ribosome since this is where mRNA and tRNAs bind (see Fig. 4 for the locations of mRNA and tRNAs).

Fig. 2 shows the 30S structure in the same view, color-coded according to the fluctuations exhibited in mode 1. The motion in mode 1 is the counter-rotation of the head against the body, accompanied by the bending of the head. The approximate rotational axis of the head and body are shown in the figure. The rotational axis of the body almost coincides with the helix 44, the penultimate stem, shown in yellow. This stem is functionally important. In the 70S assembly, this stem forms several inter-unit bridges. The top end of this stem near the neck is where the mRNA and the anticodon loop of tRNAs bind. In this mode, the shoulder is extremely immobile (blue) in contrast to other modes where the shoulder is somewhat mobile. The open space between the shoulder, beak, and the neck is where the EFs and the downstream part of the mRNA bind. The area between the neck and the platform is where the upstream mRNA comes in and wraps around the neck of the 30S on the interface side. The counter-rotation of the head against the body in mode 1 is primarily driven by the swing of the beak. In the other modes, the body and the head bend toward each other with a combination of counter-rotation.

The 30S subunit binds the mRNA first and initiates its binding to the large ribosome subunit when it finds the start codon. So the 30S subunit must be able to move along the mRNA by itself. The motions we see here can be envisioned to aid that process. The opening and closing between the head and body may help to clutch/release the mRNA. The counter-rotation of the head with respect to the body may aid in the translation of the mRNA around its neck.

3.2. The motions of the 50S subunit

We also performed ANM analysis on the 50S subunit structure reported by Yusupov et al. (PDB code 1GIY) by itself. Fig. 3A presents the structure of the 50S subunit viewed from the interface color-coded according to the deformation energy, again averaged over the 10 slowest modes. The important structural units are the L1 stalk, L7/L12 stalk, and the center protuberance (CP). The two stalks are like two arms, and the CP is like the head connected to the body. The two stalks and the CP are found by GNM/ANM (not shown) to be very mobile and their relative motions against each other and against the body comprise the first few slowest modes. For example, in mode 1, only the L1 stalk is mobile and it moves toward the CP. In mode 2, we see the L1 and L7/L12 stalks move out of the plane of the page, and the CP moves in the opposite direction.

Calculation of the flexibility on the 50S subunit with the FIRST software is performed on a different structure, 50S ribosome from *H. marismortui* (PDB code 1JJ2), the only 50S structure having atomic details. Some of the structural units are missing in this PDB file due to disorder in the crystal structure. Therefore comparison of flexible regions predicted by the two methods on the 50S ribosome subunit is somewhat complicated. In spite of this, a number of common features can be identified by comparing (A) and (B) of Fig. 3. The most flexible regions in Fig. 3A are the three peripheral structural components: the L1 stalk, the CP region, and the L7/L12 stalk. The structure analyzed by FIRST lacked the proteins and RNA loop that forms

Fig. 1. Predictions of flexibility of the ribosome 30S subunit (PDB code: 1J5E) by ANM and FIRST. The most flexible regions in the ribosome are shown by colored space-filling spheres in both panels. (A) Structure is color-coded according to the deformation energy calculated in ANM averaged over the first 10 slow modes. Red has the highest deformation energy and blue has the lowest deformation energy. The structure is viewed from the 50S interface. The landmarks shown on the structures are: head, beak, platform, and shoulder. The structure contains two dynamic domains: the head and the body, the head being somewhat more rigid than the body. (B) Predictions by FIRST. The blue backbone trace gives the largest stressed (rigid and over-constrained) cluster, which spans the entire 30S subunit while the gray backbone trace indicates regions that are flexible relative to this over-constrained cluster. The space-filling spheres show the most flexible regions. Using the PDB numbering, colored regions contain the following residues: red (80–90), cyan (1443–1451), orange (1395–1402, 1443–1451), yellow (962–971), pink (1206–1213), violet (993–998, 1003–1007, and 1026–1047), and green (1126–1143). One should note that the beak region (violet) is shown to be one of the most flexible regions as well as the red spur region, which are consistent with ANM predictions. Additional large flexible regions (yellow and orange) lie at the interface between the head and body domain and may be involved in the binding or function of mRNA. This figure was created using VMD (Humphrey et al., 1996).

Fig. 2. The motions of the 30S subunit alone in the first mode. Residues are color-coded according to the fluctuations calculated in the first mode (red is most mobile and blue is the least mobile) and the structure is in the same view as in Fig. 1. The black lines are the approximate rotational axis for the head and body. The penultimate helix 44 is shown in yellow, closely aligned with the major rotation axis. In this mode, the head counter-rotates against the body.

Fig. 3. Flexibility in the 50S subunit predicted by ANM and FIRST. (A) Prediction by ANM on the structure of the 50S subunit from *Thermus thermophilus* (PDB code: 1GIY), viewed from the 30S interface. Residues are color-coded according to the deformation energy averaged over the 10 slowest modes. The landmarks on the structures are: center protuberance (CP), L1 stalk, L7/L12 stalk, and the body. There are four dynamic domains: L1 stalk, L7/L12 stalk, CP, and the body. (B) Prediction by FIRST on the structure of the 50S subunit from *H. marismortui* (PDB code 1JJ2). The largest stressed (over-constrained) cluster is shown by a blue trace. This largest stressed cluster forms a rigid core within the structure upon which other rigid and flexible regions may move. The most flexible regions, shown by various colors, are violet (1167–1197), green (2669–2677, 2655–2657, and 2906–2914), brown (1942–1973), black (117–136), light green (2129–2136), cyan (363–372), yellow (703–725), orange (962–969), red (2330–2354), and pink (1–9 from the 5S rRNA). The location of the central protuberance (CP) is indicated as well as the L7/L12 stalk on the right. The missing L1 stalk would attach to the flexible light green region in this structure. This figure was created using VMD (Humphrey et al., 1996).

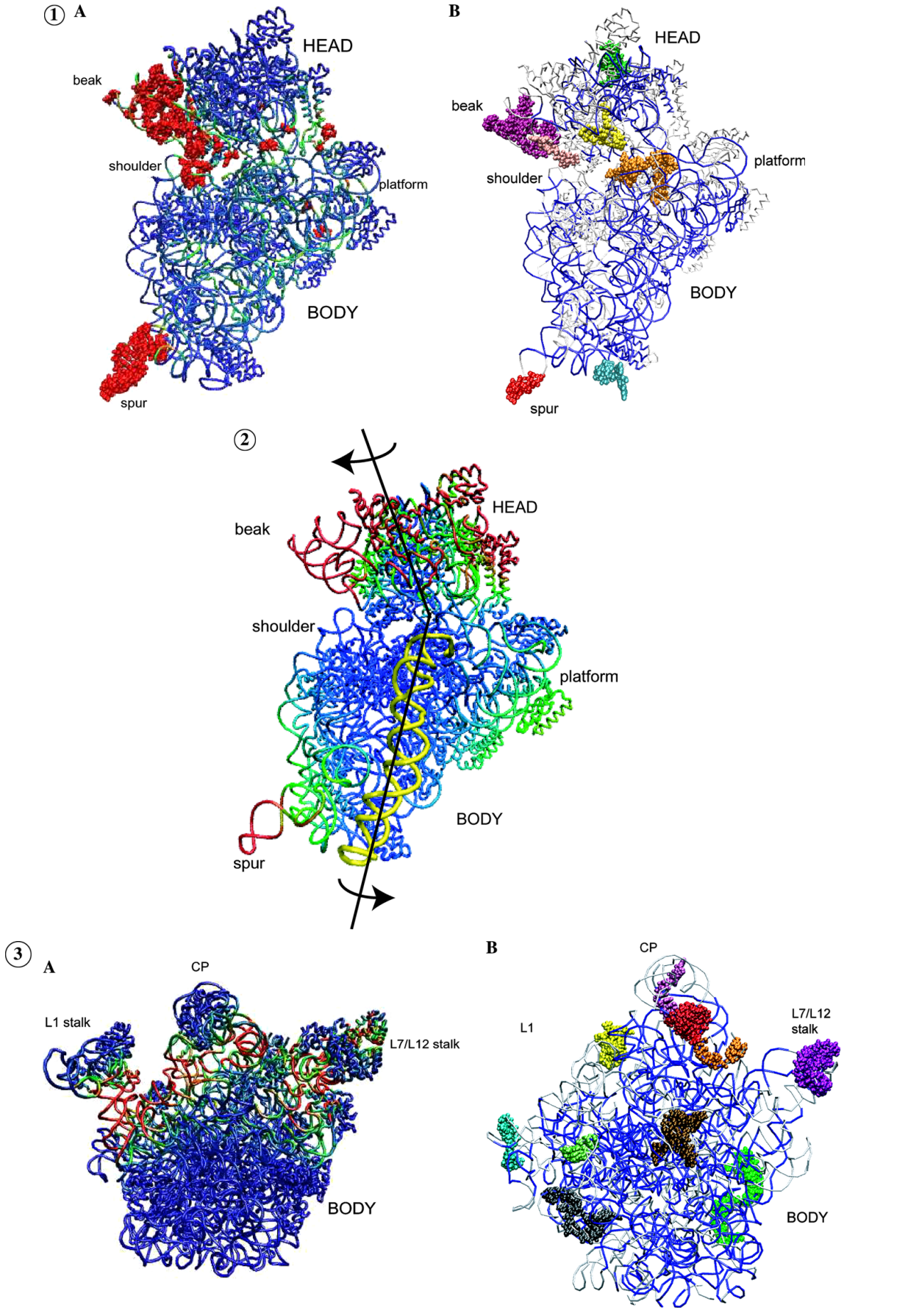
1
A
HEAD
beak
shoulder
platform
BODY
spur
B
HEAD
beak
shoulder
platform
BODY
spur
2
HEAD
beak
shoulder
platform
BODY
spur
3
A
CP
L1 stalk
L7/L12 stalk
BODY
B
CP
L1
L7/L12
stalk
BODY

the L1 stalk, however, the cyan and yellow flexible regions in Fig. 3B indicate a persistent flexibility on that side of the structure. The CP region contains the tail of the 5S rRNA indicated in pink. The CP region is attached to the rigid bulk (blue) of the 50S ribosome by two highly flexible regions (red and orange) indicating that it is probably highly mobile. The violet cluster in the L7/L12 stalk region indicates another highly flexible set of residues supporting the deformation energy calculations using ANM.

The flexibility analysis of the 30S and 50S subunits showed that the 50S ribosome subunit is more rigid than its 30S ribosome counterpart. Repeating the calculations for the 50S ribosome without its accompanying proteins resulted in a very fragmented structure supporting the experimental claim that these proteins serve to stabilize the structure to a large degree, although their catalytic roles may not be completely ruled out (Ban et al., 2000).

3.3. The motions of the 70S unit

The structure of 70S ribosome from *T. thermophilus* reported by Yusupov et al. contains the large 50S subunit, the small 30S subunit, and three tRNAs at the A, P, and E sites with a short mRNA bound. One of the proteins, L9 of the large subunit sticks out by itself in the reported structure. We first performed the calculation on the assembly including the L9 protein, but the motions of the L9 protein were so large as to dominate the motions of the remainder of the structure. There were hardly any motions in the rest of the assembly. Therefore, we have expeditiously removed the highly mobile L9 protein from further calculations.

Calculations of the deformation energy in the 70S assembly averaged over the 10 slowest modes showed clearly that the deformable residues are mostly located at the interface. Fig. 4 illustrates the view of the two subunits and the tRNAs in the 70S assembly color-coded according to the deformation energy. The three tRNAs that dock between the two subunits are strongly deformed, especially the arms that connect between the two subunits. Some of the sites on the 50S and 30S subunits, which were not deformed in Figs. 1A and 3A but revealed to be flexible by the FIRST atomic analysis (B in Figs. 1 and 3), are now found to be deformed in Fig. 4. Sites on the platform and the top of the head of the 30S subunit, and sites on the lower right end of the body and on the top of CP of the 50S are such noteworthy cases. These sites either form the bridges or are near the sites that form the bridges between the two subunits. These show that the two subunits form separate dynamic domains moving relative to each other. A recent study compared the differences between the atomic positions from low resolution cryo-EM density maps of the 70S ribosome in two different functional states (Gao et al., 2003) related by a ratchet-like motion. Comparison of the two resulting atomic models shows that the ribosome changes from a compact structure to a loose one, coupled with the re-arrangement of many of the proteins, especially those making the inter-subunit bridges. This was in agreement with our predictions of the deformation energy and flexibility calculations.

The deformation pattern of the 30S subunit in Fig. 1A differs quite significantly from that in Fig. 4A, whereas the 50S subunit in the assembly, Fig. 4B, seems to retain many of the deformation patterns observed in Fig. 3A. The spur of the 30S subunit, which was strongly deformed in Fig. 1, is now no longer deformed. The beak of the 30S subunit is also less deformed in the assembly. In contrast, the deformation patterns around the two stalks of the 50S subunit in Figs. 3A and 4B are very similar. The two stalks are again found to be very mobile. The deformation pattern around the CP is somewhat modified. The lower left edge below the CP in Fig. 4B is relatively less deformed, because the three tRNAs are docked below the CP in the assembly. The close similarity in the deformation pattern in Figs. 3A and 4B indicate that the structural units of the 50S subunit play a more important role in defining the dynamics of the assembly than the structural units of the 30S subunit.

The first few slow motions of the entire ribosome are of major interest because of their potential connection with the translocation movements within the ribosome. Experimental studies by cryo-EM have observed a ratchet-like motion (Frank and Agrawal, 2000). The 30S subunit was observed to rotate counter-clockwise (viewed from the 30S solvent side) when the EF-G binds, reducing the opening between the CP and L1 stalk and bifurcating the L7/L12 stalk. Animations of the motions along the slow modes found in our study, available at http://ribosome.bb.iastate.edu/70SnKmode, reveal that the first four slow modes all include a counter-rotation of the two subunits. Among these, mode 3 resembles the experimentally reported ratchet-like motion most closely. Panels (A) and (C) in Fig. 5 illustrate the deformed conformations of the 70S assembly in comparison to the equilibrium state (B) driven by mode 3. When the two stalks pull toward the CP (A), the 30S subunit rotates counter-clockwise viewed from the 30S solvent side. The L7/L12 stalk also undergoes a large conformational change. This large conformational change in the L7/L12 stalk may account for the bifurcation observed in the cryo-EM. The study by Tama et al. also reported that mode 3 resembled the experimentally observed ratchet-like motion (Tama et al., 2003). However, we have seen a much more significant re-arrangement of the L7/L12 stalk in this mode than they do, although we are aware that the amplitudes of the motion along the normal mode are not the same in the two studies. Another difference is the motion in mode 1. Their mode 1 had only the motion of L1 stalk, while our mode 1 included a counter-rotation of the two subunits and the motions of the two stalks.

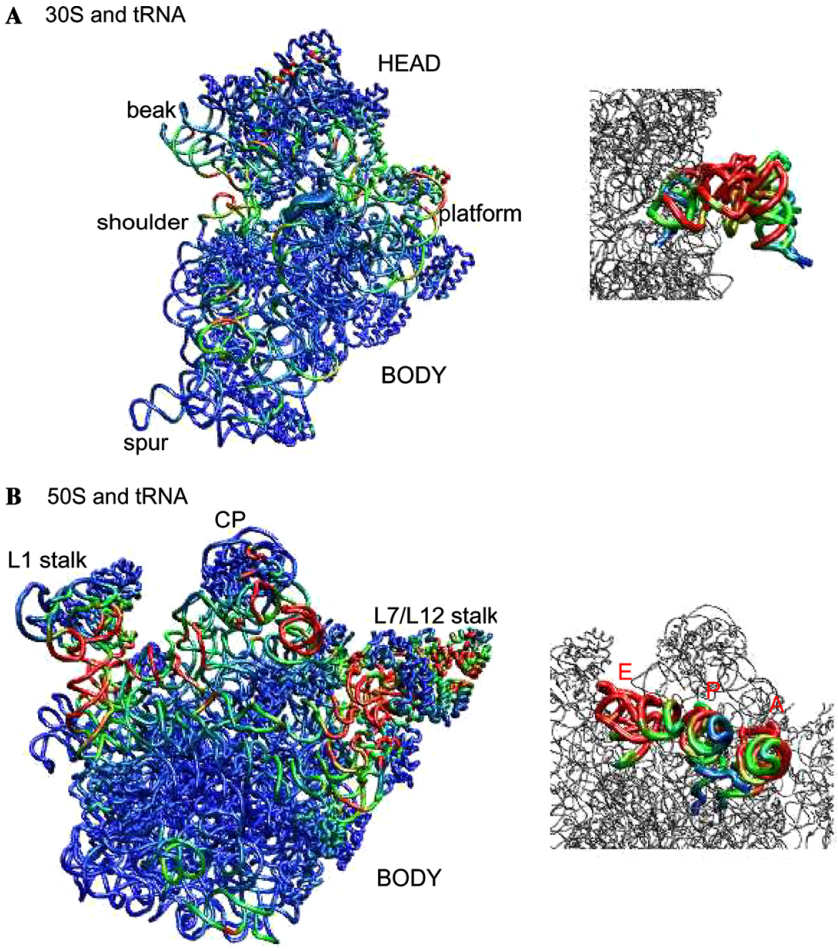

Fig. 4. The structure of the 70S assembly color-coded according to the deformation energy averaged over the 10 slowest modes. Deformable residues are mostly at the interface and on the tRNAs. The two subunits are presented separately in the interface view: (A) 30S subunit and the tRNAs, (B) 50S subunit and the tRNAs. The mRNA, which is not strongly deformed, is shown as a thick blue tube on the 30S. The view of tRNAs in the 30S subunit is rotated by 90° from the interface view.

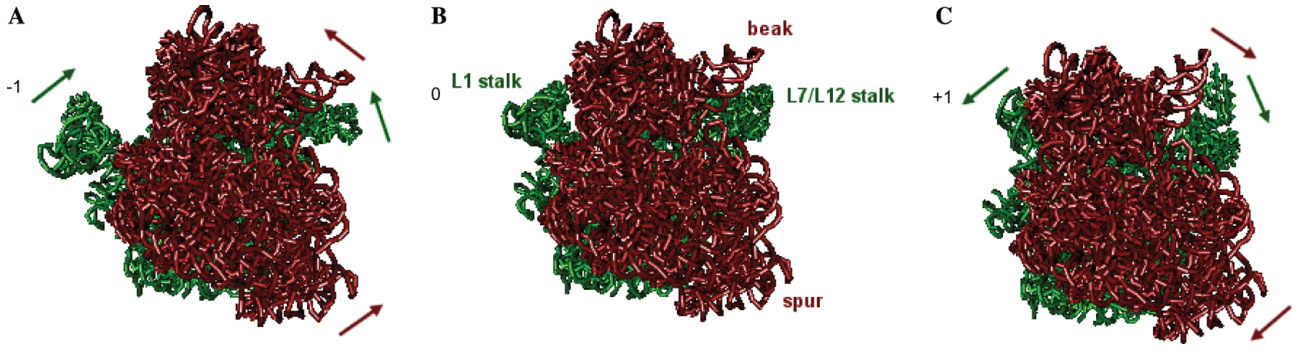

Fig. 5. The motion of the 70S assembly viewed from the 30S solvent side in ANM mode 3. The 30S subunit is shown in red and the 50S subunit in green. (A) Deformed structure at one extreme (−1) of motion; (B) original structure with no displacement (0), and (C) deformed structure at the other extreme of the motion (+1). For visualization the amplitude of the motion has been amplified by a factor of 200 over the normalized fluctuation vector. The arrows show the direction of motion away from the deformed state towards the original structure. A counter-clockwise rotation of the 30S subunit against the 50S subunits (viewed from the 30S solvent side) is accompanied by the pulling of the two arms of the 50S subunits toward the CP (−1) and vice versa (+1). The animation of this mode can be found at http://ribosome.bb.iastate.edu/70SnKmode.

Panels (A)–(C) in Fig. 6 illustrate the motion of the 70S assembly in mode 1. In this mode, the 30S subunit rotates counter-clockwise against the 50S subunit when the two stalks on the 50S subunit pull away from the CP, in the opposite direction as in mode 3. The amplitude of motion of the L1 stalk is less than that in mode

3. Moreover, the head of the 30S and the L1 stalk move in the same direction in this mode, consequently the motion of the L1 stalk is hardly distinguishable in the figure. If one examines the same motion from the right angle looking at the interface between the 30S and 50S subunit, one can see that in mode 1 the two interface closes on the right side (the L7/L12 stalk side) when the 30S rotates counter-clockwise. Mode 3 on other hand does not close as the 30S rotates. Mode 2 also has such a counter-rotation, but in mode 2, as the 30S rotates counter-clockwise, the interface between the 30S and 50S on the right side opens up, opposite to the motion in mode 1. In mode 4, the motion of the 30S unit is similar to that in mode 3, but the L1 stalk moves in the opposite direction. It moves away from the CP as the 30S rotates counter-clockwise. In higher modes, for example, in mode 6, one sees the head of the 30S subunit and the CP of the 50S subunit open up. Also we see the head of the 30S subunit and body of the 30S subunit squeeze toward each other in mode 10. Thus, a wide variety of correlated motions within the structure are evident.

3.4. Relative motions of the structural subunits in the 70S assembly

The motions of the 70S unit can be better understood when we examine the relative motions of each structural subunit. We first examine the orientation correlation between the center of mass of the displacement of the structural subunits. We sum up all the displacement vectors of sites on each structural subunit and obtain the center of mass displacements $\Delta\vec{R}_I^{\mathrm{cm}}(k)$ (note the sites are assumed to have the same mass) for each mode k, I stands for the structural subunits (30S, 50S, the tRNAs at sites A, P, and E, and the mRNA). Then we calculate the orientation correlation between the two displacement vectors by

$$C_{IJ}(k) = \frac{\Delta\vec{R}_I^{\mathrm{cm}}(k) \cdot \Delta\vec{R}_J^{\mathrm{cm}}(k)}{\left|\Delta\vec{R}_I^{\mathrm{cm}}(k)\right|\left|\Delta\vec{R}_J^{\mathrm{cm}}(k)\right|}. \tag{6}$$

The orientation can be averaged over a representative subset of modes using the weighted sum

$$\langle C_{IJ}\rangle = \Sigma_k[C_{IJ}(k)/\lambda(k)]/\Sigma_k\lambda(k)^{-1}, \tag{7}$$

when $\langle C_{IJ}\rangle$ is a positive number close to +1, the motions of two structural subunits are correlated, i.e., they move in the same direction. If it is a negative number near −1, then the two structural subunits are anti-correlated, i.e., they are coupled but move in opposite directions. If $\langle C_{IJ}\rangle$ is close to zero, the two structural subunits are either not correlated or their motions are perpendicular to one another.

Table 1 presents the orientation correlation between the subunits averaged over the 100 slowest modes. One can see that the motions of the 30S and 50S subunits are strongly anti-correlated. This could be either from counter-rotation or from opening and closing between the two subunits. The motions of 30S and 50S subunits are not much correlated with the motions of the three tRNAs (or, more likely, their motions are always perpendicular to each other) but have strong correlation with the mRNA. The 30S and mRNA are positively correlated; whereas the 50S and mRNA are anti-correlated. This indicates that the mRNA will likely move in the same direction as the 30S subunit, and in the opposite direction to the 50S subunit. In addition, the A-tRNA and the P-tRNA are strongly and positively correlated with each other, but they are less correlated with the E-tRNA. A strong correlation between the A-tRNA and the P-tRNA indicates that the A-tRNA and the P-tRNA move together in the same direction. This may indicate that the translocation of the A-tRNA to the P-site and the translocation of the P-tRNA to the E-site are likely to occur simultaneously. However, we see that the E-tRNA motion is not so strongly correlated with either the A-tRNA or the P-tRNA, but still somewhat more strongly correlated with its neighboring P-site tRNA than with the A-site tRNA. Therefore, it seems that the exit of the E-tRNA from the E-site may occur more or less independently of the translocation of the other two tRNAs. It is also worth remarking that the correlations among the tRNAs and the mRNA are all positive, indicating an overall coordination in the direction that is required for the overall processing of the mRNA.

When the ribosome is viewed from the 30S solvent side, as presented in Figs. 5 and 6, the mRNA runs horizontally from left to right around the neck of the 30S subunit. The three L-shaped tRNAs are docked

Table 1
Correlation of motions between the center of mass of the structural subunits in ribosome averaged over 100 slowest modes (PDB file: 1GIX + 1GIY)[a]

	50S	A-tRNA	P-tRNA	E-tRNA	mRNA
30S	−0.987	−0.061	−0.099	−0.066	0.498
50S		−0.006	0.025	−0.010	−0.545
A-tRNA			0.772	0.165	0.422
P-tRNA				0.313	0.386
E-tRNA					0.188

[a] Structure used was reported by Yusupov et al. (2001).

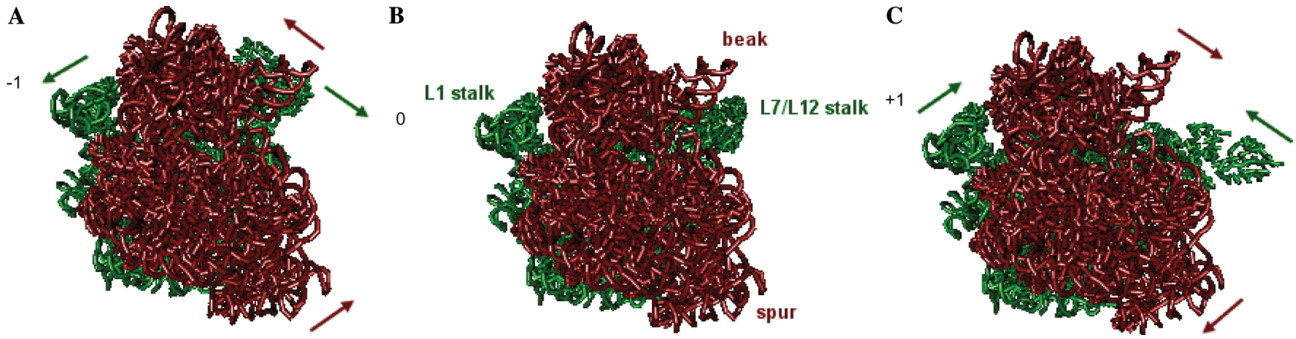

Fig. 6. The motion of the 70S assembly in mode 1 using the same color scheme as in Fig. 5, (A) deformed structure at one extreme (−1), (B) original structure (0), and (C) deformed structure at the other extreme (+1). The amplitude of the motion has been amplified by 200 times over the normalized fluctuation vector. In this mode, the 30S subunit rotates counter-clockwise against the 50S subunits (viewed from the 30S solvent side) as the two arms on the 50S subunit pull away from the CP. The 30S and 50S also close up on the right side as the 30S rotates. The animations of this mode can be found at http://ribosome.bb.iastate.edu/70SnKmode.

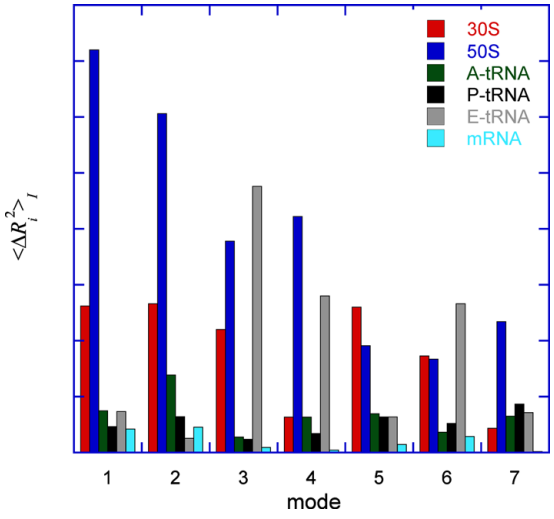

Fig. 7. Amplitude of motions induced by the first seven slowest modes on the indicated structural subunits, $\langle \Delta R_i^2 \rangle_I$ averaged over the residues forming these structural subunits. The 50S and 30S subunits show especially large displacements in the slowest modes (smallest mode indices). Also the E-site tRNA exhibits large displacements in modes 3, 4, and 6.

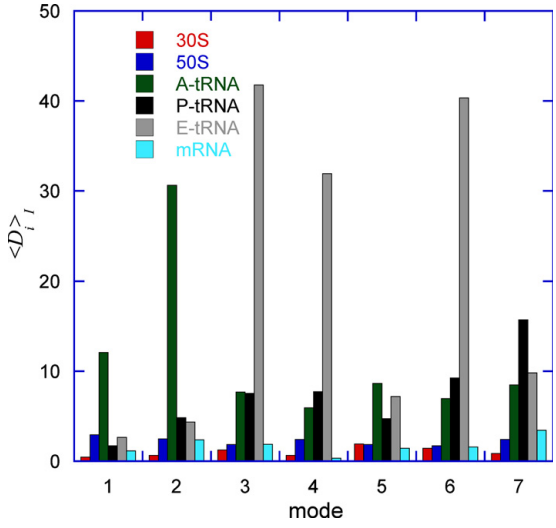

Fig. 8. Deformation energy per site, including all close interactions within the ribosome, averaged over the residues belonging to each structural subunit in the seven slowest modes. The 30S and 50S subunits have small values for all modes. The A-tRNA shows the largest values in modes 1 and 2, the E-tRNA shows the largest values in modes 3, 4, and 6, and the P-tRNA has the largest value in mode 7.

between the two subunits. The anticodon ends of the tRNAs point toward the viewer in this view and are paired with the message RNA. The 3′-ends of the tRNAs (carrying amino acid group) point downward

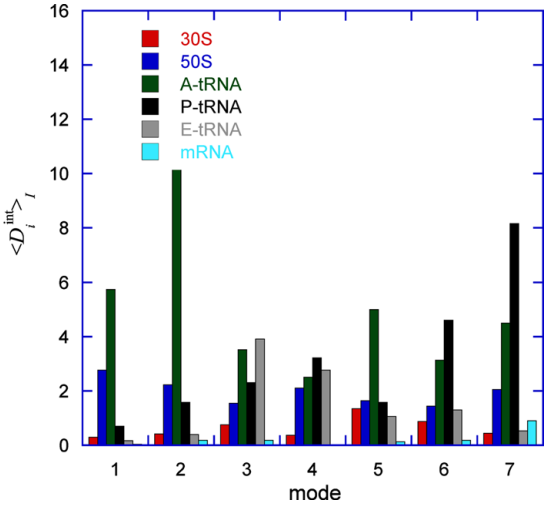

Fig. 9.

Fig. 9. Internal deformation energy per site, including only close interactions within the structural subunits, averaged for sites on each structural subunit in the seven slowest modes. Interactions between sites on different groups (30S, 50S, A-tRNA, P-tRNA, E-tRNA, and mRNA) are not included. The differences between the corresponding values in Figs. 8 and 9 reveal whether the deformation is a result of deformation of the structural subunit alone or a result of the inter-structural subunit movements. The large peaks for E-tRNA in modes 3, 4, and 6 in Fig. 8 are no longer present in Fig. 9, indicating that deformation in the E-tRNA is primarily a result of the inter-structural subunit movements, the exit of E-tRNA from the assembly.

and interact with the 50S subunit (see Fig. 4). The A-site tRNA is the most rightward, followed by the P-site tRNA, and the E-site tRNA which is the most leftward. We will see that the motions of the A-tRNA, P-tRNA, and E-tRNA differ from each other due to their different locations in the interface.

Fig. 7 compares the displacement amplitude $\langle \Delta R_i^2 \rangle_I$ per residue averaged over all the residues in each structural subunit, computed for each of the seven slowest modes. The amplitudes for each mode are weighted by the eigenvalue $\lambda(k)$, therefore the amplitude decreases with the mode index. In most of these modes, the 50S has the largest displacement amplitude, and this is primarily due to the motions in the two stalks, particularly the L7/L12 stalk. The three tRNA and the mRNA have small displacements in modes 1 and 2, but in modes 3, 4, and 6, the E-tRNA shows quite large movements. As we will show later, in these modes E-tRNA could be pushed out of the assembly. The amplitude of motion for the mRNA remains small in all of these modes, but the distribution of amplitude versus the mode number for mRNA spreads to many higher modes.

Fig. 8 compares the deformation energy $\langle D_i \rangle_I$ corresponding to each structural subunit, averaged over the residues that form the structural subunit. The sum of D_i over all sites remains constant since we are using a weighted $D_i(k)$. The distribution $D_i(k)$ over sites i reveals the relative deformability in sites. It is interesting to note that although the 30S and the 50S have large displacement amplitudes, their average deformation energies $\langle D_i \rangle_I$ are low in all these modes. This is consistent with the notion that 30S and 50S exhibit mostly rigid body motions. In contrast, the three tRNAs have relatively large deformation energy. These tRNAs serve like bridges connecting the two subunits. When the two subunits move, the tRNAs are deformed. In modes 1 and 2, the A-tRNA is distinguished by a large deformation energy. This is due to the opening/closing motion between the 30S and 50S subunits on the right side as the 30S rotates, with the A-tRNA is being squeezed or pulled as a result. In modes 3, 4, and 6, on the other hand, the E-tRNA exhibits the largest deformation energy. This is, however, not due to the compression of the E-tRNA, but largely due to the inter-subunit movements. This is further confirmed when we compute the internal deformation energy.

Internal deformation energy D_i^{int} is computed according to Eq. (5) but with the sum over j running over only the sites that belong to the same structural subunit, and not over neighboring sites on the other structural subunits. Internal deformation energy therefore is a measure of the deformation of the structural subunit itself. The difference between D_i^{int} and D_i then reflects whether the deformation has its origin in the inter-subunit movements or is due to the deformation of the structural subunit. Fig. 9 presents the internal deformation energy for each structural subunit in the first seven modes. For all structural subunits, the internal deformation energy D_i^{int} is smaller than D_i because D_i^{int} only accounts for deformation caused by residues on the same structural subunit and does not include interactions with residues on the other structural subunits. However, one can notice that in modes 1 and 2, the A-tRNA still has the largest deformation energy, the same trend as in Fig. 8. This further confirms that in modes 1 and 2, the A-tRNA is being deformed. In modes 3, 4, and 6, the large peaks for E-tRNA from Fig. 8 are no longer present in Fig. 9. This indicates that the deformation in the E-tRNA is primarily a result of the inter-subunit movement. One knows that the E-site tRNA must exit from the assembly during the translocation step. Therefore, one may conclude that this exiting of the E-tRNA might occur in modes 3, 4 or 6.

The evidence for the inter-subunit dependence of the motion for the E-tRNA is clear, but it is not so clear for the A-tRNA, the P-tRNA or the mRNA. For example, the P-tRNA has the largest amplitude of motion in mode 7, but in this mode the deformation energy and internal deformation energy for the P-tRNA are also large. In the translocation step, the A-tRNA and the P-tRNA need to move by only one codon. The extent of inter-subunit motion needed for the A-tRNA and the P-tRNA are not as large as for the E-tRNA to leave the assembly. Further analysis of the relative motions of these structural subunits will add in more understanding of the translocation steps. In particular we plan to analyze the pairwise interdependences of the deformation energies, in order to identify the connections between the deformations of the tRNAs in each mode. In addition models with the EFs will be built to attempt to understand their effects on the ribosome motions.

4. Conclusion

We have presented an initial study of the cooperative motions of the ribosome using an elastic network model GNM/ANM. The normal modes of motion are determined and analyzed for their potential links with the translocation steps known to occur in the ribosome. Several modes exhibit a counter-rotation of the 30S subunit opposite in direction to that of the 50S subunit. Specifically mode 3 resembles the experimentally reported ratchet-like motion the best. We have identified modes 3, 4, and 6 in which the E-tRNA undergoes the largest deformations and by which it will likely be able to exit from the assembly. By analyzing the correlation of the motions between the structural subunits, we have shown that motions of the A-tRNA and the P-tRNA are strongly and positively correlated. Therefore, their translocations are likely to occur simultaneously. The

E-tRNA on the other hand is not so strongly correlated with the P-tRNA and even less so with the A-tRNA. Therefore, the exit of the E-tRNA from the E-site may occur more or less independently of the translocation of the other two tRNAs. This information can be helpful in mapping out the motions of the translocation mechanism in the ribosome. Needless to say, further study and analysis of these motions are required to develop a detailed mechanism of the translocation steps in ribosome.

This study also presents a brief comparison of two methods, the elastic network model ANM, and the molecular graph theory FIRST, that have been used to predict the flexibility of the ribosome subunits. These two methods use different approaches that are expected to give a complementary view of the flexibility of the structure. Indeed, we have observed consistent predictions of some of the flexible regions on the ribosome subunits by the two methods. In particular, both methods predict that sites around the neck of the 30S subunit have intrinsic flexibility, which must be required by its capability to bind the mRNA and the tRNAs. Independent results from FIRST based on the full atomic description of the subunits validate predictions of flexibility by ANM, once again demonstrating the simple elastic network model to be a powerful tool for studying the global motions of large assemblages.

Acknowledgments

This research is partially supported by NIH (Grant No. 2S06 GM08019-29A1) and Iowa State University. The computer resource provided by North Carolina Super Computer Center is also acknowledged.

References

Agrawal, R.K., Heagle, A.B., Penczek, P., Grassucci, R.A., Frank, J., 1999. EF-G-dependent GTP hydrolysis induces translocation accompanied by large conformational changes in the 70S ribosome. Nat. Struct. Biol. 6, 643–647.

Agrawal, R.K., Spahn, C.M., Penczek, P., Grassucci, R.A., Nierhaus, K.H., Frank, J., 2000. Visualization of tRNA movements on the *Escherichia coli* 70S ribosome during the elongation cycle. J. Cell Biol. 150, 447–460.

Atilgan, A.R., Durell, S.R., Jernigan, R.L., Demirel, M.C., Keskin, O., Bahar, I., 2001. Anisotropy of fluctuation dynamics of proteins with an elastic network model. Biophys. J. 80, 505–515.

Bahar, I., Jernigan, R.L., 1999. Cooperative fluctuations and subunit communication in tryptophan synthase. Biochemistry 38, 3478–3490.

Bahar, I., Atilgan, A.R., Erman, B., 1997a. Direct evaluation of thermal fluctuations in proteins using a single-parameter harmonic potential. Fold. Des. 2, 173–181.

Bahar, I., Erman, B., Haliloglu, T., Jernigan, R.L., 1997b. Efficient characterization of collective motions and interresidue correlations in proteins by low-resolution simulations. Biochemistry 36, 13512–13523.

Bahar, I., Atilgan, A.R., Demirel, M.C., Erman, B., 1998. Vibrational dynamics of folded proteins: significance of slow and fast motions in relation to function and stability. Phys. Rev. Lett. 80, 2733–2736.

Bahar, I., Erman, B., Jernigan, R.L., Atilgan, A.R., Covell, D.G., 1999. Collective motions in HIV-1 reverse transcriptase: examination of flexibility and enzyme function. J. Mol. Biol. 285, 1023–1037.

Ban, N., Nissen, P., Hansen, J., Moore, P.B., Steitz, T.A., 2000. The complete atomic structure of the large ribosomal subunit at 2.4 Å resolution. Science 289, 905–920.

Carter, A.P., Clemons, W.M., Brodersen, D.E., Morgan-Warren, R.J., Wimberly, B.T., Ramakrishnan, V., 2000. Functional insights from the structure of the 30S ribosomal subunit and its interactions with antibiotics. Nature 407, 340–348.

Doruker, P., Jernigan, R.L., Bahar, I., 2002. Dynamics of large proteins through hierarchical levels of coarse-grained structures. J. Comput. Chem. 23, 119–127.

Frank, J., Agrawal, R.K., 2000. A ratchet-like inter-subunit reorganization of the ribosome during translocation. Nature 406, 318–322.

Frank, J., Heagle, A.B., Agrawal, R.K., 1999. Animation of the dynamical events of the elongation cycle based on cryoelectron microscopy of functional complexes of the ribosome. J. Struct. Biol. 128, 15–18.

Gao, H., Sengupta, J., Valle, M., Korostelev, A., Eswar, N., Stagg, S.M., Van Roey, P., Agrawal, R.K., Harvey, S.C., Sali, A., Chapman, M.S., Frank, J., 2003. Study of the structural dynamics of the *E. coli* 70S ribosome using real-space refinement. Cell 113, 789–801.

Haliloglu, T., Bahar, I., Erman, B., 1997. Gaussian dynamics of folded proteins. Phys. Rev. Lett. 79, 3090–3093.

Hayward, S., Berendsen, H.J., 1998. Systematic analysis of domain motions in proteins from conformational change: new results on citrate synthase and T4 lysozyme. Proteins 30, 144–154.

Hayward, S., Kitao, A., Berendsen, H.J., 1997. Model-free methods of analyzing domain motions in proteins from simulation: a comparison of normal mode analysis and molecular dynamics simulation of lysozyme. Proteins 27, 425–437.

Hinsen, K., 1998. Analysis of domain motions by approximate normal mode calculations. Proteins 33, 417–429.

Hinsen, K., Thomas, A., Field, M.J., 1999. Analysis of domain motions in large proteins. Proteins 34, 369–382.

Humphrey, W., Dalke, A., Schulten, K., 1996. VMD: visual molecular dynamics. J. Mol. Graph. 14, 33-8, 27-8.

Isin, B., Doruker, P., Bahar, I., 2002. Functional motions of influenza virus hemagglutinin: a structure-based analytical approach. Biophys. J. 82, 569–581.

Jacobs, D.J., Rader, A.J., Kuhn, L.A., Thorpe, M.F., 2001. Protein flexibility predictions using graph theory. Proteins 44, 150–165.

Keskin, O., Bahar, I., Flatow, D., Covell, D.G., Jernigan, R.L., 2002a. Molecular mechanisms of chaperonin GroEL–GroES function. Biochemistry 41, 491–501.

Keskin, O., Durell, S.R., Bahar, I., Jernigan, R.L., Covell, D.G., 2002b. Relating molecular flexibility to function: a case study of tubulin. Biophys. J. 83, 663–680.

Krebs, W.G., Alexandrov, V., Wilson, C.A., Echols, N., Yu, H., Gerstein, M., 2002. Normal mode analysis of macromolecular motions in a database framework: developing mode concentration as a useful classifying statistic. Proteins 48, 682–695.

Kundu, S., Melton, J.S., Sorensen, D.C., Phillips Jr., G.N., 2002. Dynamics of proteins in crystals: comparison of experiment with simple models. Biophys. J. 83, 723–732.

Lynch, S.R., Gonzalez, R.L., Puglisi, J.D., 2003. Comparison of X-ray crystal structure of the 30S subunit–antibiotic complex with NMR structure of decoding site oligonucleotide–paromomycin complex. Structure 11, 43–53.

Ma, J.P., Karplus, M., 1997. Ligand-induced conformational changes in ras p21: a normal mode and energy minimization analysis. J. Mol. Biol. 274, 114–131.

Marques, O., Sanejouand, Y.H., 1995. Hinge-bending motion in citrate synthase arising from normal mode calculations. Proteins 23, 557–560.

Noller, H.F., Yusupov, M.M., Yusupova, G.Z., Baucom, A., Cate, J.H., 2002. Translocation of tRNA during protein synthesis. FEBS Lett. 514, 11–16.

Rader, A.J., Hespenheide, B.M., Kuhn, L.A., Thorpe, M.F., 2002. Protein unfolding: rigidity lost. Proc. Natl. Acad. Sci. USA 99, 3540–3545.

Schluenzen, F., Tocilj, A., Zarivach, R., Harms, J., Gluehmann, M., Janell, D., Bashan, A., Bartels, H., Agmon, I., Franceschi, F., Yonath, A., 2000. Structure of functionally activated small ribosomal subunit at 3.3 angstroms resolution. Cell 102, 615–623.

Tama, F., Brooks, C.L., 2002. The mechanism and pathway of pH induced swelling in cowpea chlorotic mottle virus. J. Mol. Biol. 318, 733–747.

Tama, F., Gadea, F.X., Marques, O., Sanejouand, Y.H., 2000. Building-block approach for determining low-frequency normal modes of macromolecules. Proteins 41, 1–7.

Tama, F., Wriggers, W., Brooks, C.L., 2002. Exploring global distortions of biological macromolecules and assemblies from low-resolution structural information and elastic network theory. J. Mol. Biol. 321, 297–305.

Tama, F., Valle, M., Frank, J., Brooks, C.L., 2003. Dynamic reorganization of the functionally active ribosome explored by normal mode analysis and cryo-electron microscopy. Proc. Natl. Acad. Sci. USA 100, 9319–9323.

Temiz, N.A., Bahar, I., 2002. Inhibitor binding alters the directions of domain motions in HIV-1 reverse transcriptase. Proteins 49, 61–70.

Tirion, M.M., 1996. Large amplitude elastic motions in proteins from a single-parameter, atomic analysis. Phys. Rev. Lett. 77, 1905–1908.

Valle, M., Sengupta, J., Swami, N.K., Grassucci, R.A., Burkhardt, N., Nierhaus, K.H., Agrawal, R.K., Frank, J., 2002. Cryo-EM reveals an active role for aminoacyl-tRNA in the accommodation process. EMBO J. 21, 3557–3567.

VanLoock, M.S., Agrawal, R.K., Gabashvili, I.S., Qi, L., Frank, J., Harvey, S.C., 2000. Movement of the decoding region of the 16S ribosomal RNA accompanies tRNA translocation. J. Mol. Biol. 304, 507–515.

Wimberly, B.T., Brodersen, D.E., Clemons Jr., W.M., Morgan-Warren, R.J., Carter, A.P., Vonrhein, C., Hartsch, T., Ramakrishnan, V., 2000. Structure of the 30S ribosomal subunit. Nature 407, 327–339.

Word, J.M., Lovell, S.C., Richardson, J.S., Richardson, D.C., 1999. Asparagine and glutamine: using hydrogen atom contacts in the choice of side-chain amide orientation. J. Mol. Biol. 285, 1735–1747.

Wriggers, W., Schulten, K., 1997. Protein domain movements: detection of rigid domains and visualization of hinges in comparisons of atomic coordinates. Proteins 29, 1–14.

Wriggers, W., Agrawal, R.K., Drew, D.L., McCammon, A., Frank, J., 2000. Domain motions of EF-G bound to the 70S ribosome: insights from a hand-shaking between multi-resolution structures. Biophys. J. 79, 1670–1678.

Yusupov, M.M., Yusupova, G.Z., Baucom, A., Lieberman, K., Earnest, T.N., Cate, J.H., Noller, H.F., 2001. Crystal structure of the ribosome at 5.5 Å resolution. Science 292, 883–896.